Proc. Natl. Acad. Sci. USA
Vol. 95, pp. 7854–7859, July 1998
Physics

Stable relativistic/charge-displacement channels in ultrahigh power density ($\approx 10^{21}$ W/cm^3) plasmas

A. B. BORISOV*†, J. W. LONGWORTH*‡, K. BOYER*, AND C. K. RHODES*†§

*Department of Physics (M/C 273), University of Illinois, 845 West Taylor Street, Chicago, IL 60607-7059; †Center for Tsukuba Advanced Research Alliance (TARA), University of Tsukuba, 1-1-1 Tennodai, Tsukuba, Ibaraki 305, Japan; and ‡Department of Physics, Illinois Institute of Technology, Chicago, IL 60616

Communicated by Charles H. Townes, University of California, Berkeley, CA, May 8, 1998 (received for review February 27, 1998)

ABSTRACT **Robust stability is a chief characteristic of relativistic/charge-displacement self-channeling. Theoretical analysis of the dynamics of this stability (*i*) reveals a leading role for the eigenmodes in the development of stable channels, (*ii*) suggests a technique using a simple longitudinal gradient in the electron density to extend the zone of stability into the high electron density/high power density regime, (*iii*) indicates that a situation approaching unconditional stability can be achieved, (*iv*) demonstrates the efficacy of the stable dynamics in trapping severely perturbed beams in single uniform channels, and (*v*) predicts that $\approx 10^4$ critical powers can be trapped in a single stable channel. The scaling of the maximum power density with the propagating wavelength λ is shown to be proportional to λ^{-4} for a given propagating power and a fixed ratio of the electron plasma density to the critical plasma density. An estimate of the maximum power density that can be achieved in these channels with a power of $\approx$2 TW at a UV (248 nm) wavelength gives a value of $\approx 10^{21}$ W/cm^3 with a corresponding atomic specific magnitude of $\approx$60 W/atom. The characteristic intensity propagating in the channel under these conditions exceeds 10^{21} W/cm^2.**

The development of methods for the compression of power in materials is one of the oldest endeavors of mankind with an origin that predates the Stone Age. From the use of a wooden club to the contemporary production of vigorous thermonuclear environments, the achievable power density (W/cm^3) has been advanced by approximately a factor of 20 orders of magnitude ($\approx 10^{20}$). New processes, involving the nonlinear interaction of intense ($\approx 10^{18}$–10^{21} W/cm^2) fs pulses of radiation with matter, currently are being explored to enhance further the controlled production of these environments to a new ultrahigh level ($\approx 10^{19}$–10^{21} W/cm^3), a range that can approach $\approx$100 W/atom. These conditions provide new possibilities for the production and regulation of many highly energetic physical processes, including hard x-ray generation, the initiation of nuclear reactions, particle acceleration, and the fast ignition of fusion targets. The key to the production of these exceptional conditions is the stable compression of the spatial distribution of powerful ($P_0 \approx$ 1 TW–1 PW) pulses of radiation into very narrow plasma channels. Specifically, a complex mechanism, which is triggered by pulses whose power exceeds a critical value P_{cr} and involves both relativistic electron motions and the relative spatial separation of the electron and ion densities caused by the radiation pressure of the intense wave, produces the conditions necessary for channel formation. In brief (1), the ponderomotive radial displacement of the electrons and the contrasting inertial confinement of the ions cooperate to produce the two chief characteristics of the channels. They are (*i*) the refractive self-focusing action of the displaced electrons, which confines the propagating radiation, and (*ii*) the high spatial stability of the channels, the feature produced by the immobile electrostatic spine formed by the fixed ions. These narrow channels, which typically have a diameter of a few microns, represent an example of a new, largely unexplored class of strongly nonequilibrium excited matter that combines a very high energy density with a well-ordered structure.

The existence of dynamic stability is essential for the control of high power density plasmas. Of particular importance are the physical limits of stable behavior and the corresponding implications on the maximum achievable power density. The overall result of this study is that exceptionally robust stability is a chief characteristic of the relativistic/charge-displacement self-channeling mechanism. Specifically, the six key findings are: (*i*) the discovery of the leading role played by the eigenmodes in the development of stable channels, (*ii*) the evaluation of a simple technique using a longitudinal gradient in the electron density to extend the zone of stability into the high electron density/high power density regime, (*iii*) the indication that a situation approaching unconditional stability can be achieved, an outcome reflecting the well-ordered structure of the excited plasma, (*iv*) the demonstration of the efficacy of the dynamics in efficiently trapping severely spatially perturbed beams in single uniform channels, (*v*) an estimate showing that an extraordinary power density ($\approx 10^{21}$ W/cm^3) can be produced in the channels with UV radiation, and (*vi*) the prediction that $\approx 10^4$ critical powers (P_{cr}) can be trapped in a single stable channel.

Theoretical work (1) has predicted that the channeled propagation can exhibit a large domain of stability. Initial experimental studies (2–5), conducted close to the threshold condition of the channeling phenomenon (6–15), have furnished evidence supporting this conclusion. Measurements of the spatial properties of the propagation, using both x-ray (4) and Thomson (16, 17) images, have clearly established the formation of long channels of the form shown in Fig. 1. Fig. 1 illustrates a single-exposure x-ray [Xe(M), $\approx$1 keV] image of the longest channel (>50 Rayleigh ranges) that was experimentally produced in a gaseous target containing $(Xe)_n$ clusters (18) with a fs ($\approx$250 fs) UV (248 nm) pulse (19) having a peak power of $\approx$1.4 TW. The salient characteristic of the image is a long, stable, and uniform channel of high power density, the magnitude (20) of which was estimated to be $\approx 2 \times 10^{19}$ W/cm^3, or equivalently $\approx$1 W/atom. Other work (17), which examined the channeled region with images of the Thomson scattered 248 nm radiation, complemented the data shown in Fig. 1 and demonstrated that the channeling mechanism efficiently compresses the incident power into a single filament whose diameter does not exceed the resolution of the imaging system (5–6 μm), a result consistent with the corresponding theoretical (2, 4, 12) figure of $\approx$1–2 μm. The principal issues discussed herein are the determination of the conditions

The publication costs of this article were defrayed in part by page charge payment. This article must therefore be hereby marked "*advertisement*" in accordance with 18 U.S.C. §1734 solely to indicate this fact.

§To whom reprint requests should be addressed. e-mail: rhodes@uic.edu.

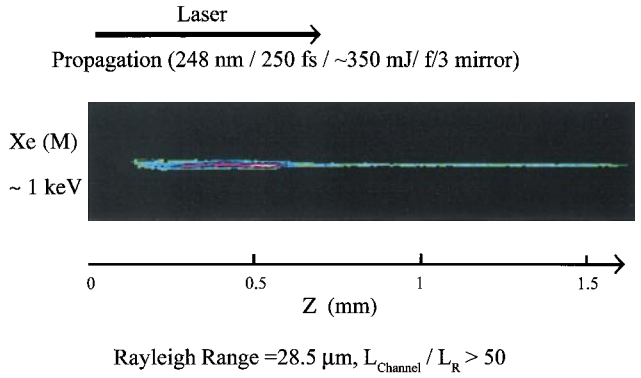

FIG. 1. Single-exposure x-ray image of a stable slender channel emitting Xe(M) radiation (≈1 keV) produced in a gaseous target containing $(Xe)_n$ clusters. The incident 248-nm pulse had a duration of ≈250 fs and an energy of ≈350 mJ, and was focused with f/3 off-axis parabolic mirror. The image was recorded with an x-ray pinhole camera having an aperture with a diameter of 25 μm and a spatial resolution of ≈30 μm. Because the Rayleigh length of the focusing system is 28.5 μm, the observed length of the channel exceeds 50 Rayleigh ranges. Additional experimental details are reported in ref. 4. The color scale (in arbitrary units) of the measured x-ray intensity is defined by black, zero; red through violet, ascending intensity; and white, maximum.

limiting the stability of the confined propagation illustrated in Fig. 1, and the evaluation of the corresponding upper bound on the power density.

Following conventional notation (1), we introduce the definitions of the coordinates of the η-ρ_0 plane given by

$$\eta = P_0/P_{cr}, \qquad \rho_0 = r_0\omega_{p,0}/c, \qquad [1]$$

with P_0 denoting the incident peak power and with the critical power (P_{cr}) given by (1, 12)

$$P_{cr} = (m_{e,0}^2c^5/e^2)\int_0^\infty g_0^2(\rho)\rho d\rho(\omega/\omega_{p,0})^2$$
$$= 1.6198 \times 10^{10}(\omega/\omega_{p,0})^2 W, \qquad [2]$$

in which $m_{e,0}$, c, and e have their customary identifications, $g_0(\rho)$ is the Townes mode (21), and ω, $\omega_{p,0}$, and r_0, are the angular frequency corresponding to the propagating radiation, the angular frequency of the unperturbed plasma, and the radius of the incident intensity profile, respectively. In addition, lowest eigenmodes (1, 10, 12) exist with the dimensionless radius

$$\rho_{e,0} = \left[2\int_0^\infty U_{s,0}^2(\rho)\rho d\rho/U_{s,0}^2(0)\right]^{1/2}, \qquad [3]$$

in which $U_{s,0}(\rho)$ represents the eigenmode (1, 10, 12) with index s. The present analysis was confined to electron densities N_e less than one-quarter of the critical electron density (N_{cr}) to eliminate resonant plasma wave production, and forward Raman scattering (22, 23) was not included, because it is known experimentally that it can be suppressed (24).

Fig. 2 illustrates the geography in the η-ρ_0 plane of the stable and unstable regions characteristic of channel formation in initially homogeneous plasmas (1). The essential features are the locus of the eigenmode curve $\rho_{e,0}(\eta)$ defined by Eq. **3**, the existence of a region of stable propagation that includes the

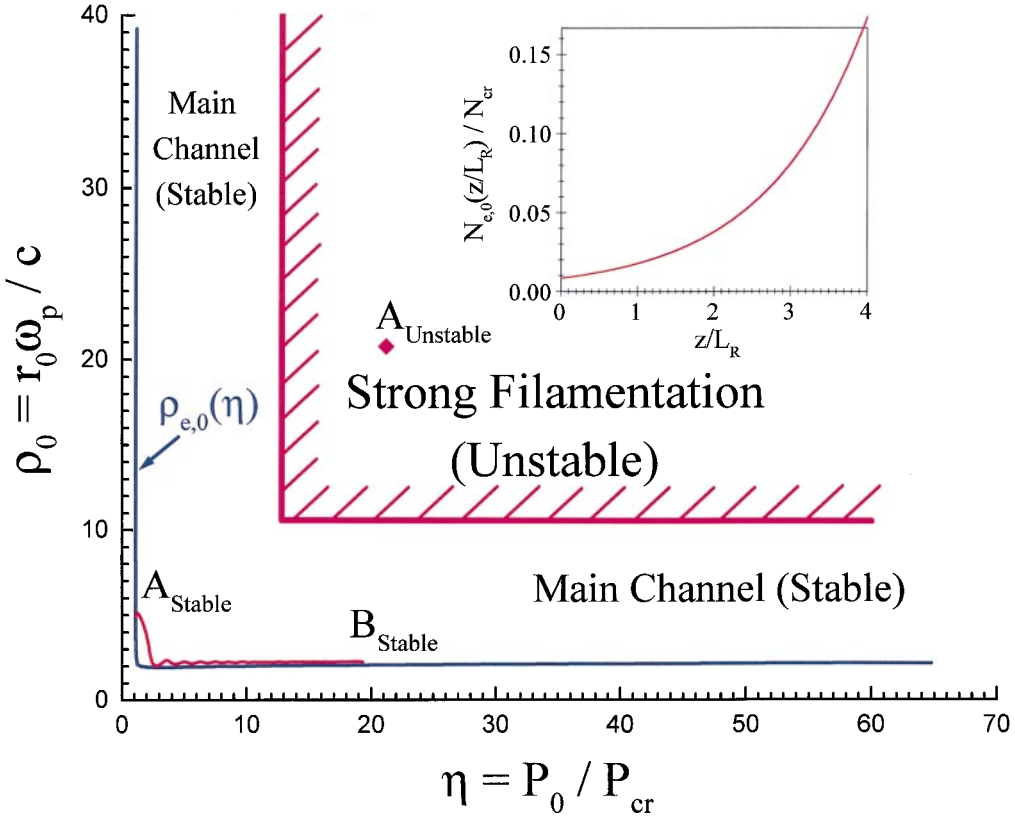

FIG. 2. Stability map in the η-ρ_0 plane for relativistic and charge-displacement self-channeling of Gaussian beams in initially homogeneous plasmas. The dimensionless coordinates ρ_0 and η are defined by Eq. **1**. Stable and unstable regions in plane (η, ρ_0) and the locus $\rho_{e,0}(\eta)$ for the lowest eigenmodes are shown. Point $A_{UNSTABLE}$ (21.1, 20.6) corresponds to the input pulse shown in Fig. 3*A*. Points A_{STABLE} and B_{STABLE} and the trajectory connecting them are described in the text. B_{STABLE} corresponds to the intensity distribution given in Fig. 3*C*. (*Inset*) The exponential longitudinal (z) electron density profile [$N_{e,0}(z) = N_{e,0}(0)\exp(\alpha z)$, $N_{e,0}(z = 3.95\,L_R) = 20\,N_{e,0}(0) = 1/6\,N_{cr}$] between points A_{STABLE} and B_{STABLE}, and L_R denotes the Rayleigh range.

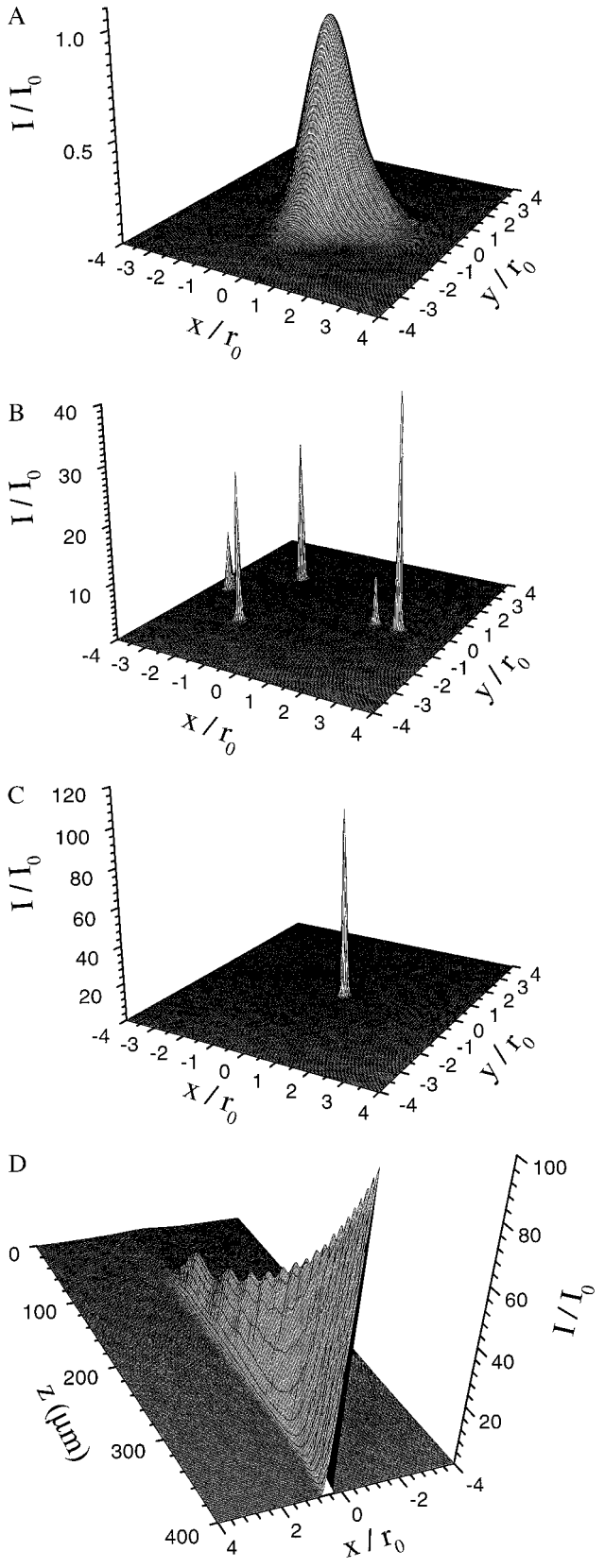

FIG. 3. Propagation characteristics of azimuthally perturbed 2 TW UV (λ = 248 nm) pulse with the parameters corresponding to data presented in Fig. 2. (*A*) The initial transverse intensity distribution (z = 0) corresponding to point A_{UNSTABLE} in Fig. 2. The azimuthally perturbed Gaussian amplitude distribution has the form $U_0(r, \phi) = I_0^{1/2}\exp(-0.5(r/r_0)^2) \times (1 + (r/r_0)^4 \Sigma\varepsilon_q \cos(q\phi))$. The distribution contains a weak azimuthal perturbation characterized by $\varepsilon_q = 0.03$, q = 1–4, and $\delta_{\mathrm{int}} = \max|I_0(r, \phi_1) - I_0(r, \phi_2)|/I_0 = 0.21$. The laser pulse and plasma parameters are λ = 248 nm, P_0 = 2 TW, r_0 = 2 μm, $I_0 = 1.59 \times 10^{19}$ W/cm^2, $N_{e,0} = 3.0 \times 10^{21}$ cm^{-3} ($N_{e,0}/N_{cr}$ = 1/6), $\eta(0)$ = 21.1, $\rho(0)$ = 20.6. (*B*) Multifocal filamentation arising from unstable propagation originating from point A_{UNSTABLE} in the case of initially uniform longitudinal electron density profile ($N_{e,0} = 3.0 \times 10^{21}$ cm$^{-3} \equiv$ const) with the initial transverse intensity distribution illustrated in *A*. The corresponding longitudinal position is $z = 3.95\, L_R$ = 400 μm and $I_0 = 1.59 \times 10^{19}$ W/cm^2. (*C*) Transverse intensity distribution of the stable channel corresponding to point B_{STABLE} in Fig. 2. The channel forms from the initial transverse intensity distribution shown in *A* in an underdense plasma with the exponential longitudinal electron density profile depicted in the inset of Fig. 2. The longitudinal position is $z_B = 3.95\, L_R$ = 400 μm and $I_0 = 1.59 \times 10^{19}$ W/cm^2. The parameters of the exponential longitudinal electron density profile are: $N_{e,0}(0) = 1.5 \times 10^{20}$ cm^{-3} and $N_{e,0}(z_B) = 3.0 \times 10^{21}$ cm^{-3} = 1/6 N_{cr}. The peak intensity in the channel is $I_{ch} = 1.62 \times 10^{21}$ W/cm^2. *C* illustrates the transverse profile of the evolved form. (*D*) Longitudinal development profile of the stable channel during evolution along the trajectory connecting A_{STABLE} and B_{STABLE} in Fig. 2. The normalized $I(x,z)/I_0$ laser intensity distribution is shown. Coordinate z represents the direction of propagation and x is one of the transverse coordinates. A single high power density channel is formed.

eigenmode curve, and a large zone of unstable propagation involving strong filamentation.

To increase the power density (W/cm^3) in the channel, both high electron density (N_e) and high radiative intensity (I) must simultaneously exist. This condition, which can be achieved by raising both the electron density (N_e) and the power (P_0) propagating in the channel, has the direct consequence of a correlated increase in both ρ_0 and η, a trend that naturally displaces the operating point of the system directly toward and eventually into the unstable zone. Therefore, the attempt to increase the power density in this straightforward manner is immediately blocked by the onset of unstable plasma dynamics. However, this limitation is overcome if there exists a mechanism maintaining the location of the operating point in the stable zone regardless of the fact that sufficiently high values of η and N_e normally exhibit unstable behavior. Analysis described below indicates that the use of an appropriate longitudinal (z) electron density gradient can achieve this goal, thereby, simply and effectively providing a large extension of the zone of stability and a corresponding major increase in the power density. Moreover, it is found that the electron density profile can be arranged in such a way that the locus of the operating point of the system becomes dynamically trapped in the stable zone by the rapid adjustment of the system to a neighborhood close to the eigenmode curve. Therefore, if the initial condition corresponds to stability, the strong dynamical preference for the eigenmode isolates the system in the stable region and the trajectory of the operating point is prevented from entering the unstable zone.

The results shown in Figs. 2–4 both illustrate the details of the propagation and provide a basis for estimating the corresponding bound on the power density. Fig. 3*A* presents an initial (z = 0) transverse intensity distribution that corresponds to point A_{UNSTABLE} (η = 21.1, ρ_0 = 20.6) in Fig. 2. Because this condition falls well within the unstable zone, the beam develops rapidly (z = 400 μm = 3.95 L_R, $L_R \equiv$ Rayleigh range) into the fragmented multichannel form shown in Fig. 3*B*.

The use of an appropriate longitudinal electron density profile, such as that given in the inset of Fig. 2, can be used to achieve the stable propagation depicted in Fig. 3*C* at both the high electron density and incident power associated with point A_{UNSTABLE} given in Fig. 2. Basically, the use of the longitudinal electron density profile shown in the inset of Fig. 2 maps the point A_{UNSTABLE} to the point A_{STABLE} in the stable zone of Fig. 2, thereby enabling the system to evolve to B_{STABLE}, the point corresponding to the intensity distribution shown in Fig. 3*C*. The profile of the pulse, as it evolves from A_{STABLE} to B_{STABLE}, is illustrated in Fig. 3*D*.

The remapping of the initial condition fundamentally alters the dynamics of the propagation. In the comparison of Fig. 3 *B* and *C*, the strongly unstable propagation in Fig. 3*B* is converted into the formation of a single stable channel that contains more than 85% of the incident power. This dramatic shift in the behavior is driven by the dynamics of the stable region, namely, the strong proclivity of the system to seek the lowest eigenmode. This characteristic of the dynamics is clearly illustrated in the form of the trajectory of the operating point in Fig. 2, which connects the initial conditions corresponding to point A_{STABLE} with the final evolved channel denoted by datum B_{STABLE}. The path of this trajectory demonstrates emphatically that the system aggressively moves toward the eigenmode and remains virtually locked in a small neighborhood of the eigenmode curve as the electron density (N_e) and corresponding value of η both rise to the conditions of high power density. This dynamical behavior contrasts sharply with other mechanisms of self-focusing (e.g., Kerr and relativistic), which generally manifest very poor characteristics of stability (11, 25, 26).

The powerful tendency for attraction to the eigenmode, illustrated by the trajectory pictured in Fig. 2, suggests that the confined propagation may be highly robust against large spatial perturbations of the incident intensity profile. To evaluate this possibility, particularly for high power ($\gg$TW) infrared (λ = 1 μm) pulses, the severely azimuthally aberrated intensity distribution of a 1 PW pulse shown in Fig. 4*A* was used to replace the weakly aberrated counterpart presented in Fig. 3*A*. The corresponding results are presented in Fig. 4 *B–D*. With the initial condition given by point A_{UNSTABLE} in Fig. 4*B*, the expected filamentation rapidly develops. However, the remapping of the launching point of the wave from A_{UNSTABLE} to A_{STABLE} with the longitudinal electron density profile depicted in the inset of Fig. 2 fully restores the stable pattern of propagation as illustrated in Fig. 4*C*. The corresponding trajectory of the operating point arising from the initial condition A_{STABLE} is illustrated in Fig. 4*B*. We note again the rapid convergence with the eigenmode curve and the efficient achievement of a single channel with the high power density corresponding to B_{STABLE}, a point representing a stable chan-

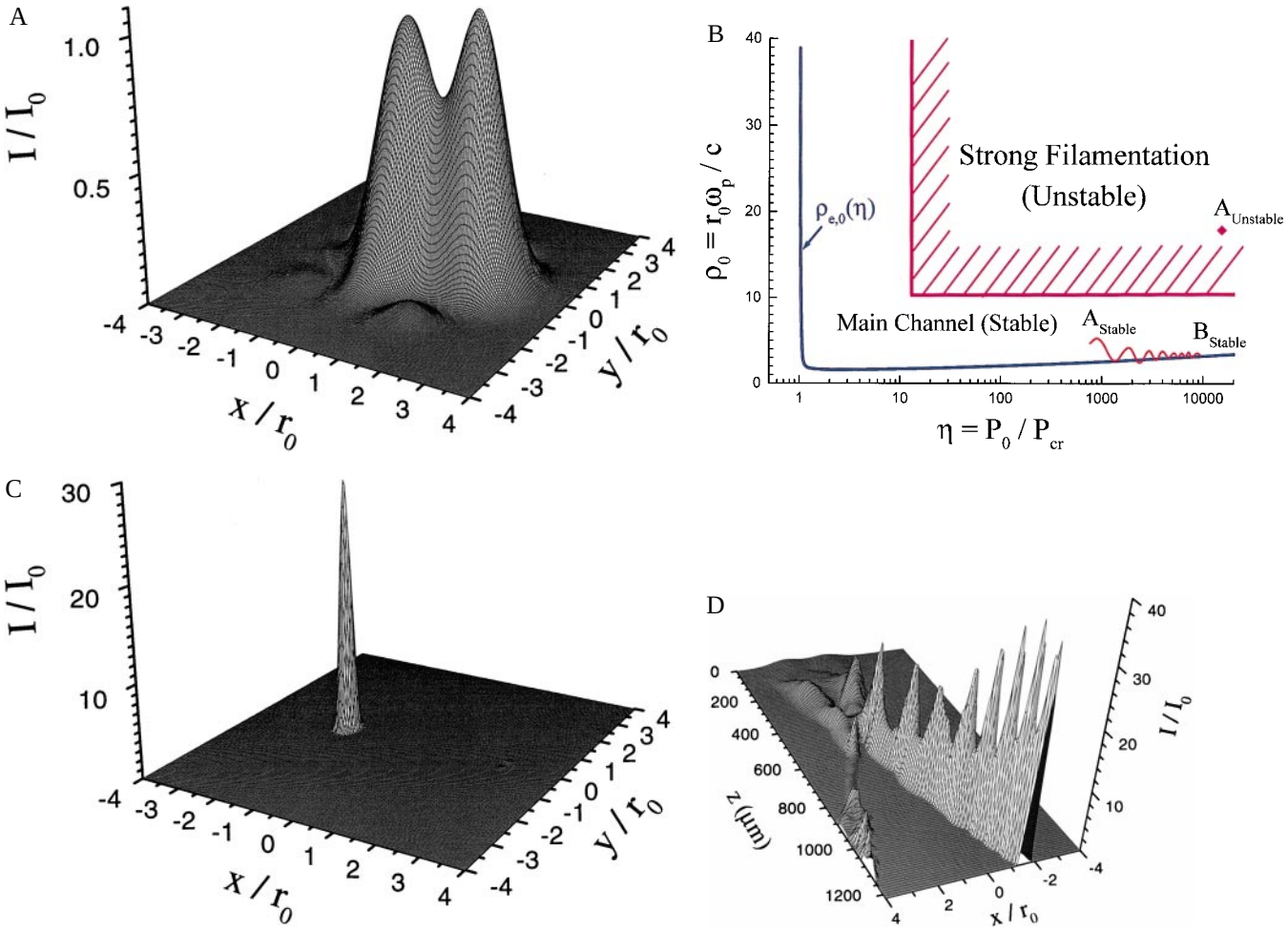

FIG. 4. Propagation characteristics of strongly azimuthally perturbed 1 PW infrared (λ = 1 μm) pulse. (*A*) Initial (z = 0) transverse (x,y) intensity distribution corresponding to point A_{STABLE} in *B*. The azimuthally perturbed Gaussian amplitude distribution has the form $U_0(r, \phi) = I_0^{1/2}\exp(-0.5(r/r_0)^2) \times (1 + (r/r_0)^4 \Sigma\varepsilon_q \cos(q\phi))$. The distribution involves a gross azimuthal perturbation characterized by ε_q = 0.1, q = 1–4, and $\delta_{\mathrm{int}} = \max |I_0(r, \phi_1) - I_0(r, \phi_2)|/I_0 = 1.06$. The laser pulse and plasma parameters are P_0 = 1 PW, λ = 1 μm, r_0 = 7 μm, $I_0 = 6.5 \times 10^{20}$ W/cm^2, $N_{e,0}(0) = 9.23 \times 10^{18}$ cm^{-3}, $\eta(0)$ = 749, $\rho(0)$ = 4.72. (*B*) Stability map in the η-ρ_0 plane that displays data corresponding to the propagation of the aberrated 1 PW, λ = 1 μm pulse. See text for details. (*C*) Transverse (x, y) intensity distribution corresponding to point B_{STABLE} in *B* showing the formation of a stable single channel. The channel forms from the initial transverse intensity distribution is shown in *A* in underdense plasma with the exponential longitudinal electron density profile depicted in the inset of Fig. 2. The longitudinal position is $z_B = 3.95\ L_R$ = 1215.2 μm, the incident peak intensity is $I_0 = 6.5 \times 10^{20}$ W/cm^2, and the corresponding electron density is $N_{e,0}(z_B) = 1.85 \times 10^{20}$ cm^{-3}, $[N_{e,0}(z_B)/N_{cr} = 1/6]$. The maximum intensity in the channel is $I_{ch} = 2.5 \times 10^{22}$ W/cm^2. *C* illustrates the transverse profile of the evolved form. (*D*) Longitudinal development profile of the stable channel during evolution along the trajectory connecting A_{STABLE} and B_{STABLE} in *B*. The normalized $I(x, z)/I_0$ laser intensity distribution is shown. Coordinate z represents the direction of propagation and x is one of the transverse coordinates.

nel containing approximately 10^4 critical powers. It is significant that the gross spatial restructuring of the pulse shown in Fig. 4*D* occurs with a modest loss of power, in this case, about 30%. The exceptional stability demonstrated by this result indicates that incident beam profiles deviating greatly from ideal spatial form can be efficiently converted into high brightness configurations.

The results discussed above provide the basis for an estimate of the upper bound of the controlled power density that can be achieved and the dependence of that limit on the wavelength (λ) of the propagating radiation. For $\lambda = 248$ nm, $N_e/N_{cr} \cong 1/6$, and an incident $P_0 = 2$ TW, it was found (cf. Fig. 3*C*) that the peak intensity in the channel is $I_{ch} \cong 1.62 \times 10^{21}$ W/cm^2. To estimate the effective cross section $\sigma_{n\gamma}$ for coupling of the radiation to the atomic or molecular material in the channel, we use a previous estimate (27) of the upper bound of $\sigma_{n\gamma}$ valid in the limit of sufficiently high intensity ($>10^{20}$ W/cm^2) and sufficiently high atomic number (Z). This analysis (27) led to a universal magnitude given by $\sigma_{n\gamma} = 8\pi \lambda\!\!\!^{-2}_c$ in which $\lambda\!\!\!^{-}_c$ is the Compton wavelength of the electron. In arriving at this value for $\sigma_{n\gamma}$, appeal was made to a picture involving an extreme form of ordered driven electronic motion in atoms (28), a model that bears an analogy to certain atom-atom and ion-atom collisional processes (29). We note that this value of $\sigma_{n\gamma}$ also has an experimental basis, because it gives good agreement (20) for power densities ($\approx$1 W/atom) derived from images of Xe x-ray spectra produced in channels (30, 31). If we further assume that the channel contains uranium atoms at an average density N_U that experience ionization to the level $Z = 70$, the state of ionization predicted at an intensity $\approx 1.7 \times 10^{21}$ W/cm^2 by the Coulomb suppression model (32), we can write the corresponding power density (P/V) approximately as

$$\frac{P}{V} \cong N_U \sigma_{n\gamma} I = \frac{N_e}{Z} \sigma_{n\gamma} I \cong 2.6 \times 10^{21} \text{ W/cm}^3, \qquad [4]$$

or equivalently $\approx$60 W/atom.

Because the self-channeling causes the transverse intensity profile of the laser beam to stabilize near a lowest eigenmode (1, 3, 12), the peak intensity I_{ch} in the channel can be expressed from Eqs. **1–3** as (1, 4)

$$I_{ch} = \left(\frac{4\pi\eta_{ch}}{\rho_{e,0}^2}\right)\left(\frac{m_{e,0}^2 c^5}{e^2\lambda^2}\right)\int_0^\infty g_0^2(\rho)\rho d\rho, \qquad [5]$$

where $\eta_{ch} = P_{ch}/P_{cr}$, and P_{ch} represents the power trapped in the channel. For the range of $1.4 \lesssim \eta_{ch} \lesssim 10$, the normalized radius of the lowest eigenmodes is nearly constant (1, 3), $\rho_{e,0} \cong 1.7$, and Eq. **5** reduces to the simple expression

$$I_{ch} = 7 \times 10^{18} \frac{\eta_{ch}}{\lambda^2} \text{ W/cm}^2 \qquad [6]$$

with λ given in units of micrometers.

The self-channeling of ultra-powerful PW laser pulses in high density plasmas generally involves a trapped power in the channel P_{ch} that is the order of 10^3–10^4 P_{cr}. For this range ($10^3 \lesssim \eta_{ch} \lesssim 4\times10^4$), the normalized radius of the lowest eigenmodes is $\rho_{e,0} \simeq 3$, and Eq. **5** for this range reads

$$I_{ch} = 2 \times 10^{18} \frac{\eta_{ch}}{\lambda^2} \text{ W/cm}^2 \qquad [7]$$

with λ given in units of micrometers.

It follows from the definition of N_{cr} that I_{ch} can be written in the form

$$I_{ch} = \frac{4\pi}{\rho_{e,0}^2}\frac{N_e}{N_{cr}} P_{ch}\lambda^{-2} = \frac{4\pi}{\rho_{e,0}^2}\frac{P_{ch}}{P_0}\frac{N_e}{N_{cr}} P_0\lambda^{-2}. \qquad [8]$$

Because both $\rho_{e,0}$ and P_{ch}/P_0 vary slowly over the range $10 \lesssim \eta_{ch} \lesssim 10^4$ ($\rho_{e,0} \approx$ const, $P_{ch}/P_0 \approx$ const), the peak intensity in the channel scales as

$$I_{ch} \sim \frac{N_e}{N_{cr}} P_0 \lambda^{-2}, \qquad [9]$$

a result, which gives for a constant ratio of N_e/N_{cr} the simple scaling

$$I_{ch} \sim P_0 \lambda^{-2}. \qquad [10]$$

From the obvious relation $N_e \approx \lambda^{-2}$ for $N_e/N_{cr} \equiv$ const, together with Eqs. **4** and **10**, we conclude that at a constant ratio of N_e/N_{cr} the power density P/V is expected to vary as

$$P/V \sim P_0 \lambda^{-4}. \qquad [11]$$

Within a margin of $\approx$10 percent, the results of our computations conform to this strong expected scaling favoring the UV.

In conclusion, detailed studies of the stability of relativistic/charge-displacement self-channeling have revealed two chief characteristics of this nonlinear mechanism of propagation: a dominant role for the lowest eigenmode for pulses launched in the stable zone and an exceptional robustness of the stability of single channels. As a consequence, strongly azimuthally perturbed incident intensity profiles can undergo efficient confinement to stable channeled distributions. The results demonstrate how a simple gradient in the electron density can be used to augment the effectiveness of the stable region and extend the channeling process into a high power-density regime that unites high propagating intensities with high plasma densities.

Support for this research was provided under contracts with the Strategic Defense Initiative/Naval Research Laboratory (N00014-93-K-2004), the Army Research Office (DAAH04-94-G-0089 and DAAG55-97-1–0310), the Department of Energy at the Sandia National Laboratories (DE-AC04-94AL85000), the University of California/Lawrence Livermore National Laboratory (B328353), and the Japanese Ministry of Education, Science, Sport, and Culture (08405009 and 08750046).

1. Borisov, A. B., Shiryaev, O. B., McPherson, A., Boyer, K. & Rhodes, C. K. (1995) *Plasma Phys. Control. Fusion* **37,** 569–597.
2. Borisov, A. B., Borovskiy, A. V., Korobkin, V. V., Prokhorov, A. M., Shiryaev, O. B., Shi, X. M., Luk, T. S., McPherson, A., Solem, J. C., Boyer, K. & Rhodes, C. K. (1992) *Phys. Rev. Lett.* **68,** 2309–2312.
3. Borisov, A. B., Shi, X. M., Karpov, V. B., Korobkin, V. V., Shiryaev, O. B., Solem, J. C., McPherson, A., Boyer, K. & Rhodes, C. K. (1994) *J. Opt. Soc. Am. B* **11,** 1941–1947.
4. Borisov, A. B., McPherson, A., Thompson, B. D., Boyer, K. & Rhodes, C. K. (1995) *J. Phys. B* **28,** 2143–2158.
5. Monot, P., Auguste, T., Gibbon, P., Jakober, F., Mainfray, G., Dulieu, A., Louis-Jacquet, M., Malka, G. & Miquel, J. L. (1995) *Phys. Rev. Lett.* **74,** 2953–2956.
6. Young, P. E., Ford, M. E., Hammer, J. H., Kruer, W. L., Tabak, M. & Wilks, S. C. (1995) *Phys. Rev. Lett.* **75,** 1082–1085.
7. Wagner, R., Chen, S.-Y., Maksimchuk, A. & Umstadter, D. (1997) *Phys. Rev. Lett.* **78,** 3125–3128.
8. Borghesi, M., MacKinnon, A. J., Barringer, L., Gaillard, R., Gizzi, L. A., Meyer, C., Willi, O., Pukhov, A. & Meyer-ter-Vehn, J. (1997) *Phys. Rev. Lett.* **78,** 879–882.
9. Malka, G., Fuchs, J., Amiranoff, F., Baton, S. D., Gaillard, R., Miquel, J. L., Pépin, H., Rousseaux, C., Bonnaud, G., Busquet, M. & Lours, L. (1997) *Phys. Rev. Lett.* **79,** 2053–2056.
10. Sun, G.-Z., Ott, E., Lee, Y. C. & Guzdar, P. (1987) *Phys. Fluids* **20,** 526–532.
11. Borisov, A. B., Borovskiy, A. V., Korobkin, V. V., Prokhorov, A. M., Shiryaev, O. B. & Rhodes, C. K. (1990) *Phys. Rev. Lett.* **65,** 1753–1756.

12. Borisov, A. B., Borovskiy, A. V., Shiryaev, O. B., Korobkin, V. V., Prokhorov, A. M., Solem, J. C., Luk, T. S., Boyer, K. & Rhodes, C. K. (1992) *Phys. Rev. A* **45,** 5830–5845.
13. Pukhov, A. & Meyer-ter-Vehn, J. (1996) *Phys. Rev. Lett.* **76,** 3975–3978.
14. Sprangle, P., Esarey, E. & Hafizi, B. (1997) *Phys. Rev. Lett.* **79,** 1046–1049.
15. Pukhov, A. & Meyer-ter-Vehn, J. (1997) *Phys. Rev. Lett.* **79,** 2686–2689.
16. Borisov, A. B., McPherson, A., Thompson, B. D., Boyer, K. & Rhodes, C. K. (1997) in *Multiphoton Processes 1996: Proceedings of 7th International Conference on Multiphoton Processes*, eds. Lambropoulos, P. & Walther, H. (IOP, Bristol), Inst. Phys. Conf. Ser. No. 154, pp. 1–9.
17. McPherson, A., Cobble, J., Borisov, A. B., Thompson, B. D., Omenetto, F., Boyer, K. & Rhodes, C. K. (1997) *J. Phys. B* **30,** L767–L775.
18. McPherson, A., Thompson, B. D., Borisov, A. B., Boyer, K. & Rhodes, C. K. (1994) *Nature (London)* **370,** 631–634.
19. Bouma, B., Luk, T. S., Boyer, K. & Rhodes, C. K. (1993) *J. Opt. Soc. Am. B* **10,** 1180–1184.
20. Borisov, A. B., McPherson, A., Boyer, K. & Rhodes, C. K. (1996) *Progr. Crystal Growth Character. Mat.* **33,** 217–223.
21. Chiao, R. Y., Garmire, E. & Townes, C. H. (1964) *Phys. Rev. Lett.* **13,** 479–482.
22. Forslund, D. W., Kindel, J. M. & Lindman, E. L. (1975) *Phys. Fluids* **18,** 1002–1016.
23. Decker, C. D., Mori, W. B., Katsouleas, T. & Hinkel, D. E. (1996) *Phys. Plasmas* **3,** 1360–1372.
24. McPherson, A., Borisov, A. B., Boyer, K. & Rhodes, C. K. (1996) *J. Phys. B* **29,** L291–L297.
25. Bespalov, V. I. & Talanov, V. I. (1966) *J. Exp. Theor. Phys. Lett.* **3,** 307–309.
26. Campillo, A. J., Shapiro, S. L. & Suydam, B. R. (1973) *Appl. Phys. Lett.* **23,** 628–630.
27. Boyer, K., Jara, H., Luk, T. S., McIntyre, I. A., McPherson, A., Rosman, R. & Rhodes, C. K. (1987) *Rev. Phys. Appl.* **22,** 1793–1799.
28. Boyer, K. & Rhodes, C. K. (1985) *Phys. Rev. Lett.* **54,** 1490–1493.
29. Briggs, J. S. & Taulbjerg, K. (1978) in *Structure and Collisions of Ions and Atoms*, ed. Sellin, I. A. (Springer, Berlin), pp. 105–153.
30. Borisov, A. B., McPherson, A., Boyer, K. & Rhodes, C. K. (1996) *J. Phys. B* **29,** L113–L118.
31. Borisov, A. B., McPherson, A., Boyer, K. & Rhodes, C. K. (1996) *J. Phys. B* **29,** L43–L50.
32. Augst, S., Strickland, D., Meyerhofer, D. D., Chin, S. L. & Eberly, J. H. (1989) *Phys. Rev. Lett.* **63,** 2212–2215.